AN ANALYSIS OF FALLING LEAF SUPPRESSION STRATEGIES FOR THE F/A-18D

Paul T. Jaramillo*
Bihrle Applied Research, Inc.
Hampton, Virginia 23666

Abstract

A large-angle simulation model for the F-18C/D has been recently validated and reported.[1-11] Utilizing this model, various methods of suppressing falling leaf motions were evaluated. The results indicated that falling leaf motions were highly susceptible to damping applied to the wind roll axis. The difficulty of implementing such a scheme is that the required states are not always measured, or measured accurately. Another suppression strategy, which performed at nearly the same level, involved applying a damping moment directly against the instantaneous angular momentum vector of the aircraft. The advantage of this system is that it requires information which is available and accurately measured on most fighter aircraft. In general, the method performed consistantly on all types of falling leaf motions and would likely be effective in oscillatory and flat spins. Comparisons between these two motion suppression schemes as well as others are presented.

Nomenclature

b	span
C_l	rolling moment coefficient
C_m	pitching moment coefficient
C_n	yawing moment coefficient
C_{damp}	damping moment increment before gain
C_{apply}	damping moment increment after gain
$\bar{c}$	mean aerodynamic chord
H	angular momentum
I_{ij}	principal moments of inertia
P	roll rate
Q	pitch rate
R	yaw rate
α	angle-of-attack
β	sideslip angle
Θ_i	generic orientation angle
Ω	total angular velocity

*Research Engineer, Member AIAA

I. Introduction

The "falling leaf" is a motion which involves large excursions in angle-of-attack and sideslip coupled with significant rotation. The changes in aerodynamic angles sometimes exceeds 100 degrees per second. Unlike a spin, the motion does not involve a continuous unidirectional heading angle change, but oscillates in roll and yaw about zero or small nonzero means. This behavior is produced by a complex interplay between dynamic and aerodynamic moments, and involves strong coupling about all axes.

The purpose of this work was to study methods for effecting recoveries from the falling leaf motions experienced by the F/A-18D. The research was undertaken in such a manner as to provide insight into the motions as well as provide a guiding philosophy for designing recovery controls. The goals of this study were:

1) determine the best control strategy for stopping falling leaf motions,
2) determine the role of the automatic flight control system during the motion, and
3) determine the probable effects of some of the aerodynamic terms.

This paper deals primarily with the first goal.

II. Overview

In order to study the robustness of all of the schemes evaluated, three simulations were employed encompassing the full range of falling leaf motions. The angle-of-attack traces of these simulations are shown in Figure 1, however a more comprehensive picture of the motions can be found in references 10 and 11. The basic idea was to apply damping moments about specific axes to impede the motion and hopefully lead to recovery. The damping was initiated at various times during each of the simulations and maintained until a recovery was effected. This would allow a realistic assessment of each control strategy's effectiveness during each specific type of falling leaf motion as well as reduce the possibility that the recovery technique was timing dependent. The use of

several simulations allowed an assessment of each strategy's effectiveness across the spectrum of falling leaf motions.

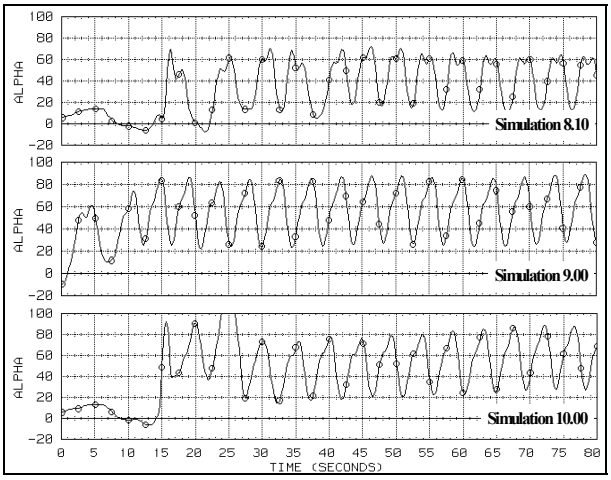

Figure 1. Angle-of-Attack Traces for the Simulations Used in the Study

Different recovery strategies were compared by measuring the amount of damping moment, in coefficient form, required to effect a 20 second recovery. For the purposes of this work, recovery was defined as a condition in which the absolute values of angle-of-attack and sideslip were less than 10 degrees occurring simultaneously with minimal rotation. The definition of recovery used in this work is one of convenience for the sake of the experiment. That is, no implication has been made that 20 seconds will be needed for recovery from a falling leaf. Faster recoveries can be achieved with most of the strategies by simply applying more damping moment; and the actual implementation of any of the strategies would presumably utilize all available control power in order to effect the fastest recoveries possible. For the reader's information, a 20 second recovery would result in about 5000 feet of altitude loss after which the aircraft would still have to level out from what was typically a 75 degree dive. Because of the 4-5 second period of each (fast) falling leaf cycle, the 20 second recovery was chosen to reduce statistical scatter in the results and therefore enhance comparisons between different strategies. With this definition, the differences in the performance between each of the strategies was plainly visible and did not require statistical metrics to compare suppression methods.

The two qualities sought after in a recovery system were 1) effectiveness during all types of falling leaf motions and 2) low damping moment requirement. The first characteristic implies strategy robustness while low damping moments are desirable because the control moments have to be attainable by the control surfaces. The second point is particularly important since the falling leaf spends the vast majority of the time at high angle-of-attack, high sideslip, or both; and control power is strongly dependent on both.

III. Test Algorithm

This section describes the algorithm used for testing various motion suppression strategies. Figure 2 provides a graphical depiction of the process to go along with the point by point description presented in this section. The specific goals of this procedure were to identify potential recovery systems for countering the falling leaf, segregate these methods by effectiveness, and identify strategies which should be avoided because they may be detrimental to the falling leaf or other out-of-control motions. A side benefit of this procedure is that it helped identify the specific effects of some of the aerodynamic increments used in the model. These increments include the control power and damping terms.

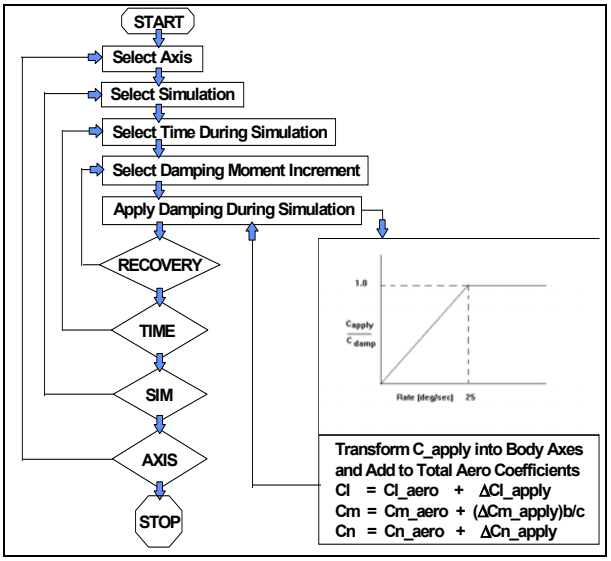

Figure 2. Flow Chart of Algorithm for Testing Motion Damping Strategies

1. Select a damping axis. This is synonymous with selecting a recovery (suppression) strategy. The cases studied are given in Table 1, which provides a brief description of each axis and the information necessary in order to implement a feedback loop for that strategy. The appendix contains a more detailed description of some of the methods and provides the necessary mathematical relations needed to develop the numerical algorithms.

Table 1. Axes About which Damping Moments Were Applied

DAMPING AXIS	NAME	DESCRIPTION	INFORMATION REQUIRED
Roll Axis	P	X-Body Axis	P
Stability Roll Axis	Pstab	Projection of Velocity Vector onto Plane-of-Symmetry	P, R α
Wind Roll Axis	Pwind	Aligned with Translational Velocity Vector	P, Q, R α, β
Yaw Axis	R	Z-Body Axis	R
Stability Yaw Axis	Rstab	Normal to Stability Roll Axis and in Plane-of-Symmetry	P, R α
Rotational Axis	Ω	Aligned with Rotational Velocity Vector	P, Q, R
Angular Momentum Axis	H	Rotational Velocity Distributed by Inertias	P, Q, R I_{ij}

2. Select a simulation. As mentioned previously, several simulations were used in this study because they represented the spectrum of falling leaf motions experienced by the aircraft. The differences between these motions is most pronounced in the angle-of-attack traces as illustrated in Figure 1. The minimum angle-of-attack is as low as -5 degrees in one motion and as high as 30 degrees in another. Nevertheless, each motion sweeps through about the same range of angles, i.e. about 60 degrees between the minimum and maximum angles-of-attack.

3. Select a time to begin recovery. In order to ensure that the recovery strategies were adequately tested on each of the types of motions, times for initiating recovery were selected typically every two to four seconds along each simulation. This provided adequate coverage of each of the types of motions to ensure that the results were consistent and representative.

4. Select a damping increment: C_damp. The value of the damping moment coefficient, C_damp, is the basis for comparing the effectiveness of different strategies. The damping increment must first be run through a gain schedule, and in some cases, transformed into components along the body axes, before it can be applied. The mathematical relations for doing this are presented in the appendix.

5. Apply damping increment, C_apply. C_apply is determined according to Figure 3. The x-axis of the graph is determined by the damping strategy, e.g. if roll damping is being tested, then the x-axis of Figure 3 is the roll rate. In effect, Figure 3 is a generic gain schedule which converts C_damp into C_apply. Some recovery strategies call for the application of damping about mathematically defined axes. Ultimately, however, the damping must be defined relative to the body axes. Coordinate transformations provided in the appendix are used to distribute C_apply back along the body axes. The transformed components are then added to the total aerodynamic moment coefficients of the aircraft's aerodynamic model as in Eq. 1. Once initiated, the damping increment is applied continuously during the simulation.

$$\begin{aligned} C_l &= C_{l\,aero} + \Delta C_{l\,apply} \\ C_m &= C_{m\,aero} + \Delta C_{m\,apply}\frac{b}{\bar{c}} \\ C_n &= C_{n\,aero} + \Delta C_{n\,apply} \end{aligned} \qquad (1)$$

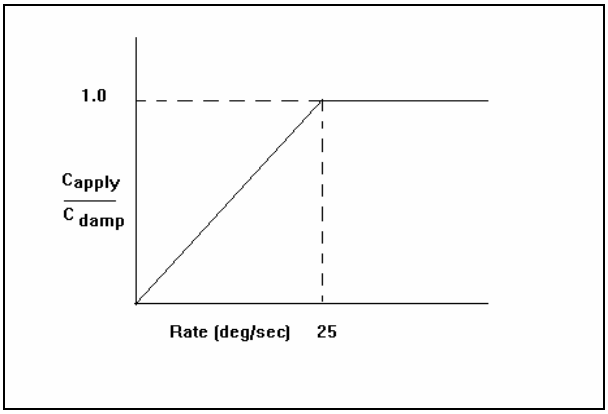

Figure 3. Schedule for Applying Damping Moments During Simulations

6. Time recovery. For the purposes of this experiment, recovery was defined as a condition with absolute values of angle-of-attack and sideslip less than 10 degrees occuring simultaneously with minimal rotation. The recovery was required to be as close as possible to 20 seconds without exceeding it. If the recovery did not equal 20 seconds, the procedure required going back to Step 4 to adjust the damping

moment coefficient, C_damp, upwards or downwards until a 20 second recovery was achieved in this step.

Figure 4 illustrates this process for a case when damping is initiated at 45 seconds. As can be seen, a damping increment of 0.01 yielded a 15 second recovery. The damping increment was then reduced to 0.006 which resulted in a 35 second recovery. This was improved to 25 seconds with a 0.007 increment. Finally, the damping increment was adjusted to 0.008 which yielded the required 20 second recovery. Once the 20 second recovery had been achieved, the axis, simulation number, time damping was initiated and the damping increment were recorded. The idea behind forcing the recovery to fit the 20 second criteria was to provide a meaningful basis of comparison between the different strategies.

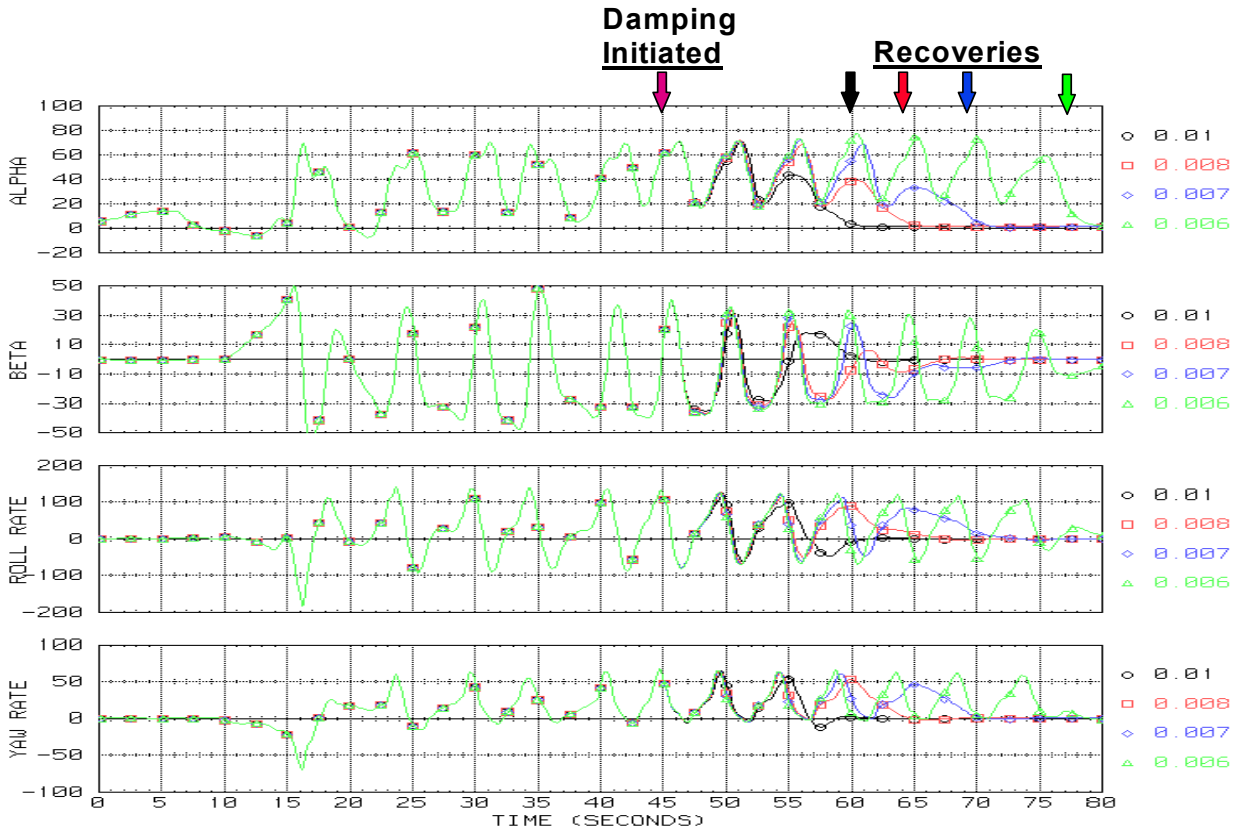

Figure 4. Determination of Recovery Moment Yielding a "20 Second Recovery"

7. Return to Step 3 and select a new time to initiate the recovery. If the selected simulation run has been adequately covered, go to to Step 8.

8. Return to Step 2 and select a new simulation. After all simulations have been used, go to to Step 9.

9. Return to Step 1 and select a new damping axis. After all axes have been evaluated, stop.

IV. Strategy Effectiveness

Figure 5 provides the data collected during the investigation. The recovery increment, C_damp, is plotted against the time during the simulations when the damping was initiated. The results for all three simulations are plotted on each graph for brevity. As mentioned, the three simulations covered the full spectrum of falling leaf motions. The reason for selecting multiple times during each simulation was simply to ensure that the performance of each strategy was fully evaluated, and possibly expose timing dependent behavior, i.e. if recovery depended on the specific time during a falling leaf cycle when the damping was initiated. In general, characteristics which should be considered desirable for a recovery system are 1) low damping moment requirement, 2) similar performance regardless of type of motion, and 3) timing independence.

Although the difference between the minimum and maximum angles-of-attack during a falling leaf cycle remains roughly constant for all types of falling leaf motions, the entire trace can shift to lower or higher values. This shift has been linked to the angular momentum of the motion and can therefore be used as

one of the means to distinguish between the different types of falling leaf motions.[11]

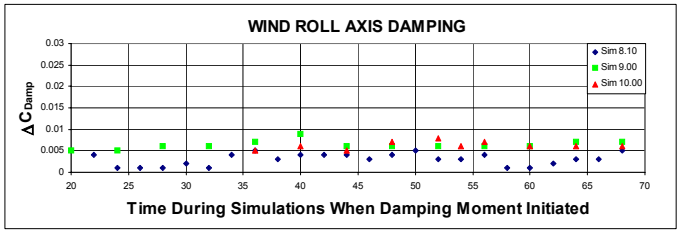

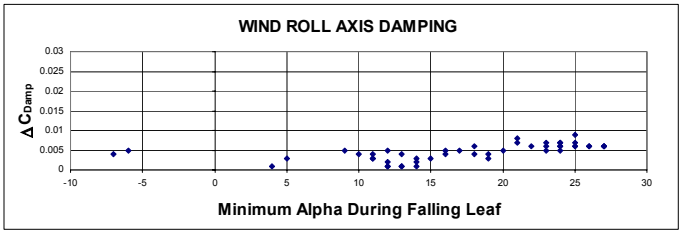

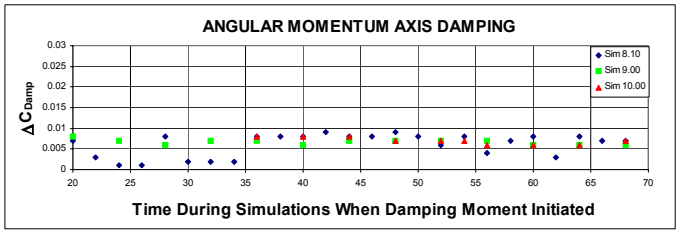

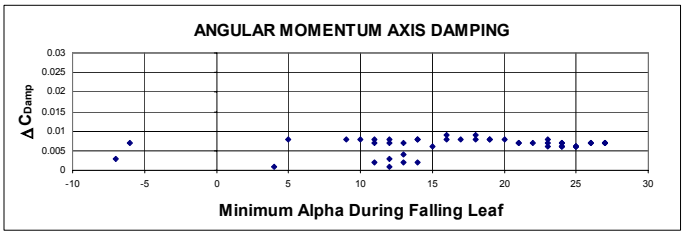

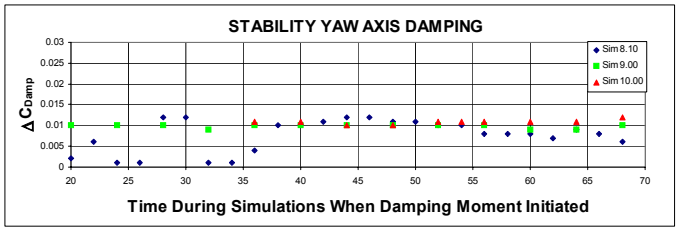

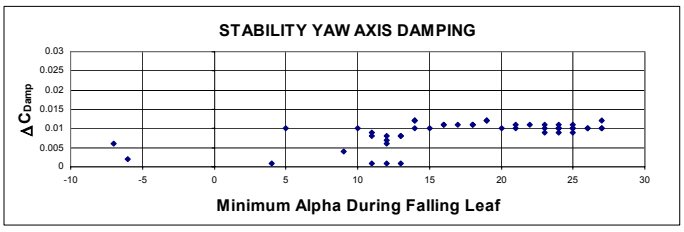

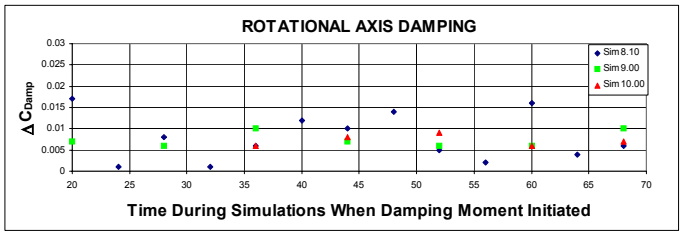

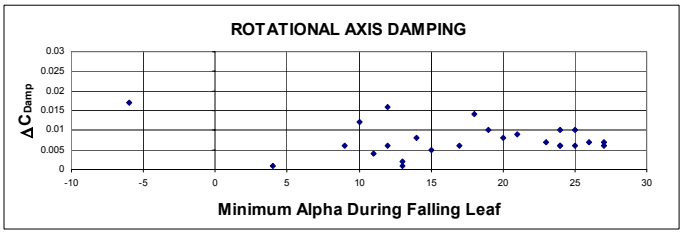

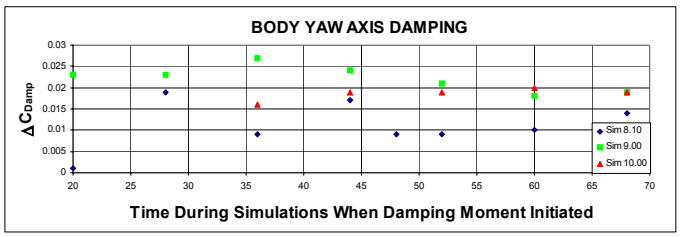

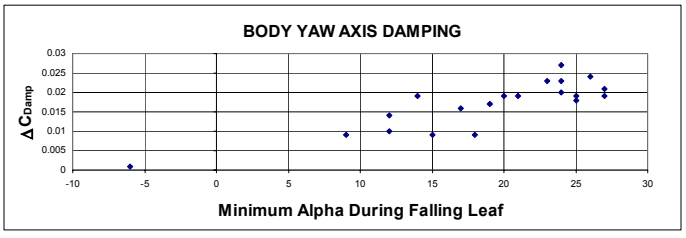

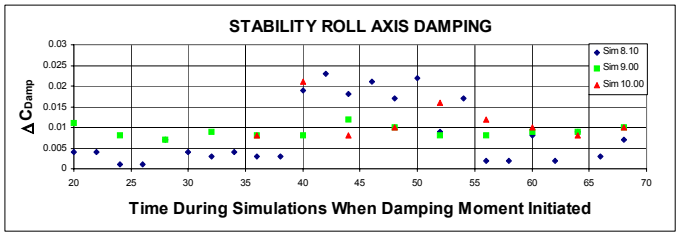

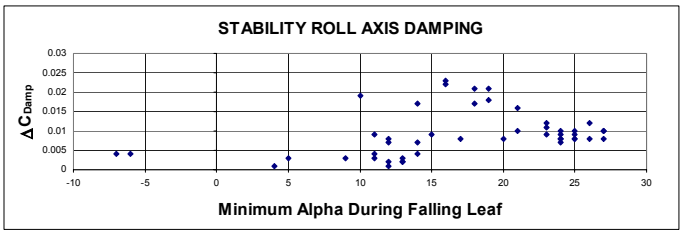

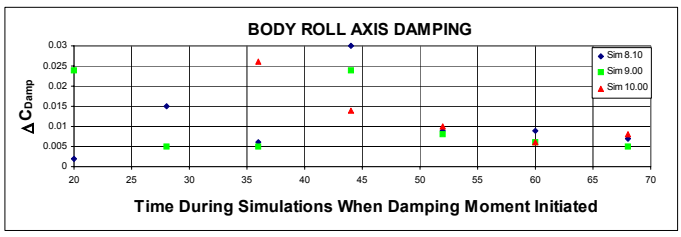

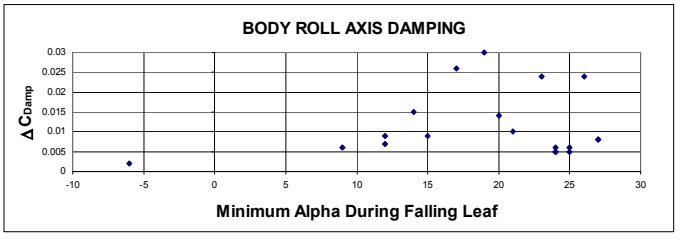

Figure 5. Effectiveness of Recovery Strategies During Several Falling Leaf Motions

Figure 6. Effectiveness of Recovery Strategies Across Falling Leaf Spectrum

By plotting the recovery moment against the minimum angle-of-attack of the motion, as is done in Figure 6, the effectiveness of each strategy across the falling leaf spectrum, could be illustrated. To do this, a spline was constructed connecting the bottoms of the angle-of-attack cycles for each of the simulations used. With these splines, the minimum angle-of-attack of the motion could be read at the instant when the damping was initiated, even if the damping was initiated at some time other than the bottom of the angle-of-attack cycle. In this way, the recovery moment, ΔC_damp could be plotted against a metric correlated to the type of motion.

Overall, the wind roll axis damping strategy required the lowest damping moments to effect recoveries across the falling leaf spectrum. The performance of this scheme can be related to its effect on the aircraft's dynamic damping increments. The first graph of Figure 6, shows that the wind axis scheme displays some dependence on the angle-of-attack range of the motion, as evidenced by an upward trend in ΔC_damp as the minimum angle-of-attack of the motion increases. Nevertheless, in general the damping requirements remained low. One drawback of the wind axis scheme is that reliable measurement of both angle-of-attack and sideslip along with all of the rotational rates, are required in order to implement this scheme. This detracts somewhat because of the lower reliability of angle-of-attack measurement and the lack of sideslip measurement on most aircraft. It is expected, however, that this strategy would remain effective in oscillatory and especially in flat spins. The latter are characterized by a superposition of the rotational and translational (wind) axes.

The momentum axis damping scheme, which apportions damping about all three axes according to the products of the angular rates and inertias of the respective axes, provided very good performance during all types of falling leaf motions. Several advantages of this scheme stand out. First, its performance was insensitive to the type of motion. Second, it required relatively low damping moments to effect recoveries. Third, the method only requires the measurement of the rotational rate components, all of which can be reliably measured. Although, the method does require the moments-of-inertia of the aircraft, indications are that the method can tolerate large errors in the values of the inertias. This can be surmised, in part, from the performance of the rotational axis damping method, which ranked fourth among the methods tested and would be equivalent to a momentum axis scheme if the inertia ratios were 1:1:1 (I_{xx}:I_{yy}:I_{zz}). As such, for this aircraft the rotational axis scheme can also be thought of as the momentum axis scheme with gross errors in the inertias (up to 500% since the inertia ratio of this aircraft is approximately 1:4:5). Finally, the momentum axis scheme is likely to maintain its effectiveness through oscillatory and steady spins because of the larger emphasis it would place on body axis yaw damping during these motions.

Stability axis yaw damping provided the third best performance. In general, it provided consistent performance across the spectrum of motions but required about 20 to 30 percent more damping moment to effect recoveries than the momentum axis scheme and almost 50 percent more than the wind axis scheme. Implementation of this scheme requires accurate measurement of angle-of-attack along with the roll and yaw rates. One area in which this method is *not* expected to be appropriate is in the area of spins, particularly flatter spins. This is because in a spin, the motion approaches a wind axes roll involving primarily body axis yawing. As a result, the stability axes yawing component, which is equivalent to the wind axes yawing component, becomes very small and in fact disappears as the spin becomes flat. In other words, in these motions, there would be nothing to feedback, and equivalently, nothing to control.

Rotational axis damping provided the median level of performance of the schemes tested. Its lower performance during some of the motions is attributed to the emphasis it places on the roll axis, which has a high velocity relative to the other axes, but holds little angular momentum due to its smaller moment-of-inertia. In the same manner, it de-emphasizes yaw rate damping due to the lower yaw rate magnitudes, even though the yaw axis contains the lions share of the momentum with its larger inertia. Another important point is the trend displayed by the rotational axis damping as the motions increased in angle-of-attack (fourth graph in Figure 6). In particular, the rotational axis damping scheme improved to the performance levels of the best schemes as the angle-of-attack of the motion increased. This is because the translational and rotational velocity vectors tend to coincide more often, meaning that wind axis and rotational axis damping tend to start operating in the same way. As such it would also be effective in flat spins.

Yaw rate damping was strongly affected by the angle-of-attack range of the motion, requiring larger moments to effect recovery as the angle-of-attack increased. All single axis damping strategies, however, performed poorly due to the strong dynamic coupling between the axes. Unlike the roll or pitch axes, the yaw axes scheme at least provided stable solutions. The increased damping moment requirement with increased

angle-of-attack is probably a direct consequence of the increased angular momentum of the motion. One trend just beginning to be displayed at the highest angles-of-attack, however, is a peak in the moment required for recovery and what appears to be the beginning of a downward trend. This result was anticipated because yaw axis damping should become the dominant means of impeding the motion as it approaches a flat spin.

Both stability- and body- axes roll damping provided the worst performance and should be avoided. Both generally required very high damping moments and the solutions were not stable during moderate angle-of-attack motions. The last two graphs of Figure 6 show that for a given time during the motion, applying progressively higher moments did not necessarily lead to a gradual decrease in recovery times. Instead, lower applied damping moments often drove the motion into a high alpha falling leaf until at some level of ΔC_damp, a recovery occurred. However, as progressively higher damping moments were applied, instead of simply yielding faster recoveries, the simulation was often driven into a different out-of-control trajectory which would not recover until extremely high, and certainly unattainable moments, had been applied.

Finally, some experimentation on pitch damping was performed but preliminary results indicated it would be an ineffective counter to the falling leaf. Furthermore, its implementation would be hampered by the fact that the horizontal stabilizer was saturating at positive deflections during the motion. Although the wind, momentum and rotational axis damping schemes call for some pitch damping, the inability to provide additional upward travel would not have a large effect on their success. This is because a large negative deflection margin was available and only a small amount of pitch damping was called for. Physically, the pitch axis is a poor candidate because of the lag in the pitch rate behind the roll and yaw rates during the motion. This results from the strong dependence of the total pitching moment on the inertial component. In essence, the pitch axis acts as a temporary storage of momentum during each falling leaf cycle.

V. Summary and Conclusions

Table 2 below summarizes the relative performance of the strategies tested. The first metric, low damping moment, is related to the attainability of the method based on availability of control power at high angle-of-attack and sideslip. Low required moments are preferred because any excess control power can be used to obtain the fastest possible recoveries. The second metric addresses the observation that several types of falling leaf motions exist. The chosen control strategy should be sufficiently robust as to be able to suppress all variations of the motion. The independence of the suppression strategy on the precise moment it is initiated indicates that the strategy is stable and robust. Some strategies gave significantly different responses when the motion suppression was initiated only a couple of seconds apart during a given simulation. This is obviously an undesirable characteristic. The fourth metric addresses the fact that some states cannot, at present, be reliably measured (the aerodynamic angles in particular). The implementation of a strategy, of course, is only as good as measurements from which it is based. Finally, the ability of a strategy to work effectively against other types of out-of-control motions, such as steady or oscillatory spins, is attractive to engineers and pilots alike.

Table 3 underlines an important feature of falling leaf type motions. Specifically, the falling leaf is a complex non-linear motion with strong lateral, directional and longitudinal motion coupling. This is evidenced by the poor performance of single axis damping systems, and the relatively good performance of three axes damping systems. The effect of this coupling is also evidenced by the mid to poor performance of the two axes systems which distribute damping along the roll and yaw axes only, and entirely neglect the effect of sideslip.

In sum, this study found that the wind roll axis damping strategy required the least damping moment to suppress falling leaf motions. However, it requires accurate measurement of the aerodynamic angles, in addition to the angular rates. An excellent alternative, which requires only the measurement of the angular velocity components and an estimate of the aircraft's inertias is the momentum axis damping scheme. Both the wind and momentum axes schemes are likely to remain effective during flat or oscillatory spins. All single axis damping methods required very high control moments while some methods, such as stability roll axis damping were unstable and should be avoided altogether.

Acknowledgments

The authors wish to express their gratitude to Bill McNamara and Chad Miller at NAWC/AD Manned Flight Simulation Facility for their support of this work.

Table 2. Summary of Effectiveness of Motion Damping Strategies

METRIC	H	Pwind	Rstab	Omega	Yaw	Roll	Pstab
Low Damping Moment Required	X	X	X				
Effective on all Types of Falling Leaf Motions	X	X	X	X			
Independent of Timing During Falling Leaf Cycle	X	X	X				
Reliability of Required State Measurements	X			X	X	X	
Probable Effectiveness on other Out-of-Control Motions	X	X		X	X		X

Table 3. Suppression Schemes Ranked by Average Damping Moment Requirement

Suppression Schemes	Number of Body Axes About Which Damping Must be Applied
Pwind (Wind Axes Roll Damping)	**3-Axes**
H (Momentum Axis Damping)	**3-Axes**
Rstab (Stability Axess Yaw Damping)	**2-Axes**
Ω (Rotational Axis Damping)	**3-Axes**
R (Yaw Damping)	**1-Axis**
Pstab (Stability Axes Roll Damping)	**2-Axes**
P (Roll Damping)	**1-Axis**
Q (Pitch Damping)	**1-Axis**

References

1. Hess, R. A., "Subsonic F/A-18A and F/A18A/B Aerodynamic Identified from Flight-Test Data," Rept No. SCT-4522-220-1, July 1987.

2. Ralston, John N., "Analysis of F-18A/B Low Speed, High Angle-of-Attack Aerodynamic Data Base, Bar 88-7, September 1988.

3. Hess, R. A., "Effect of Various Stores on the Aerodynamics of an F/A-18B Aircraft Aerodynamic Identified from Flight-Test Data," Rept No. SCT-6612-020-2, February 1989.

4. Glaser, B., Hess R. K., Trame, L. W., "F/A-18 V8.33 Control Law Mechanization," McDonnell Douglas Memo 338-5788, May 1984.

5. O'Conner, Cornelius, "NATC F-18A/B Aerodynamic Math Model Modifications Incorporated during the Phase I Model Unification Effort," BAR 89-5, March, 1989.

6. O'Conner, Cornelius, "NATC F-18A/B Aerodynamic Math Model Modifications Incorporated during the Phase II Model Unification Effort," BAR 90-13, September, 1990.

7. Ralston, John N. and Avent, J. L., "Evaluation and Modification of F/A-18B Aerodynamic Data Base for Improved Departure Modeling, BAR 92-2, Mar. 1992.

8. Ralston, John N., O'Connor, C. J. and Avent, J. L., "Evaluation of the NAWC/AD F/A-18 C/D Simulation Including Data Base Coverage and Dynamic Data Implementation Techniques," BAR 95-3, Dec. 1995.

9. O'Connor, C. J., Ralston, John N., and Timothy Fitzgerald, "Evaluation of the NAWC/AD F/A-18 C/D Simulation Including Data Base Coverage and Dynamic Data Implementation Techniques," AIAA Paper 96-3365, May 1996.

10. Jaramillo, P. T., and Ralston, J. N., "Simulation and Analysis of the F/A-18D Falling Leaf Motion with an Assessment of Suppression Strategies," BAR 95-9, December, 1995.

11. Jaramillo, P. T., and Ralston, J. N., "Simulation of the F/A-18D Falling Leaf," AIAA Paper 96-3371, August 1996.

Appendix

This appendix provides a brief description, along with some of the math, for the different recovery strategies used in the study.

A.1 Stability Axes Roll Damping

The definition of stability axes used in this study differs somewhat from the conventional definition often used in linear systems analysis. In the conventional sense, the motion being studied begins with a reference condition which may include a reference angle-of-attack and a sideslip. The x-stability axis would be defined as the projection of the velocity vector onto the aircraft's plane-of-symmetry at the reference condition, and would remain fixed to the body during the ensuing motion. In the sense presented here, the stability axes are continually redefined by the instantaneous angle-of-attack and are not subject to remain fixed at any reference state. As such the stability axes rates are calculated by Eq. 2 below.

$$\begin{Bmatrix} P_{stab} \\ Q_{stab} \\ R_{stab} \end{Bmatrix} = \begin{bmatrix} \cos(\alpha) & 0 & \sin(\alpha) \\ 0 & 1 & 0 \\ -\sin(\alpha) & 0 & \cos(\alpha) \end{bmatrix} \begin{Bmatrix} P \\ Q \\ R \end{Bmatrix} \tag{2}$$

A damping moment is applied to oppose the stability axes roll rate according to Figure 3, with Pstab on the x-axis of the figure.

Once the applied damping moment is determined from Figure 3, it is simply transformed back into the body axes using Eq. 3 below.

$$\begin{Bmatrix} C_{l\_apply} \\ C_{m\_apply} \\ C_{n\_apply} \end{Bmatrix} = \begin{bmatrix} \cos(\alpha) & 0 & -\sin(\alpha) \\ 0 & 1 & 0 \\ \sin(\alpha) & 0 & \cos(\alpha) \end{bmatrix} \begin{Bmatrix} C_{apply} \\ 0 \\ 0 \end{Bmatrix} \tag{3}$$

A.2 Stability Axes Yaw Damping

Stability axes yaw damping utilizes Eq. (2) to determine Rstab. Again Figure 3 is used to determine the damping moment, C_apply, to be applied about the z-stability axis. Eq. 4 below is then used to transform the damping moment back into the body axes.

$$\begin{Bmatrix} C_{l\_apply} \\ C_{m\_apply} \\ C_{n\_apply} \end{Bmatrix} = \begin{bmatrix} \cos(\alpha) & 0 & -\sin(\alpha) \\ 0 & 1 & 0 \\ \sin(\alpha) & 0 & \cos(\alpha) \end{bmatrix} \begin{Bmatrix} 0 \\ 0 \\ C_{apply} \end{Bmatrix} \tag{4}$$

A.3 Wind Axes Roll Damping

The wind axis is the velocity vector. Wind axes roll damping can be performed in a manner similar to the procedures discussed in A.1 an A.2. First, wind axes roll rate is calculated using Eq. 5 below. The wind axis transformation is equivalent to the Euler angle sequence: body 231 (-α, β, 0).

$$\begin{Bmatrix} P_{wind} \\ Q_{wind} \\ R_{wind} \end{Bmatrix} = \begin{bmatrix} \cos(\alpha)\cos(\beta) & \sin(\beta) & \sin(\alpha)\cos(\beta) \\ -\cos(\alpha)\sin(\beta) & \cos(\beta) & -\sin(\alpha)\sin(\beta) \\ -\sin(\alpha) & 0 & \cos(\alpha) \end{bmatrix} \begin{Bmatrix} P \\ Q \\ R \end{Bmatrix} \tag{5}$$

The damping moment needed to oppose wind axes roll rate uses Figure 3 with Pwind on the x-axis. Then Eq. 6 below is used to transform C_apply into body axes increments.

$$\begin{Bmatrix} C_{l\_apply} \\ C_{m\_apply} \\ C_{n\_apply} \end{Bmatrix} = \begin{bmatrix} \cos(\alpha)\cos(\beta) & -\cos(\alpha)\sin(\beta) & -\sin(\alpha) \\ \sin(\beta) & \cos(\beta) & 0 \\ \sin(\alpha)\cos(\beta)) & -\sin(\alpha)\sin(\beta) & \cos(\alpha) \end{bmatrix} \begin{Bmatrix} C_{apply} \\ 0 \\ 0 \end{Bmatrix} \tag{6}$$

One note of caution is that the pitch increment, Cm_apply as given by Eq. 6 is not defined in the customary manner. In particular, since it is the actual moment (a vector) which is being transformed, all of the coefficients have to be non-dimensionalized by the same scalar quantities. For example, if C_apply is assumed to be non-dimensionalized by dynamic pressure, area and span, then so are the transformed coefficients (left-hand side of equation). Thus the applied pitching increment, Cm_apply must be multiplied by: b/c in order to bring it into customary form and allow it to be added to the total pitching moment coefficient of the aero-model.

A.4 Rotational Axis Damping

The rotational axis is the rotational velocity vector of the aircraft. A simple way to determine its orientation is to define a convenient Euler angle sequence. Eq. 7 below provides such a means which utilizes definitions analogous to the angle-of-attack and sideslip.

$$\begin{aligned} \Omega &= \sqrt{P^2 + Q^2 + R^2} \\ \Theta_1 &\equiv \tan^{-1}\left(\frac{R}{P}\right) \quad . \; . \; . \; . \quad -\pi < \Theta_1 \le \pi \\ \Theta_2 &\equiv \sin^{-1}\left(\frac{Q}{\Omega}\right) \quad . \; . \; . \; . \quad -\frac{\pi}{2} < \Theta_2 \le \frac{\pi}{2} \end{aligned} \tag{7}$$

With these angles, an orthogonal transformation from the body axes to the newly defined rotational axes can be determined. For convenience, the Euler angle sequence is also defined analogous to the wind axis transformation, i.e. body 231 ($-\Theta_1$, Θ_2, 0). This is provided in Eq. 8 below.

$$\begin{Bmatrix} P_\Omega \\ Q_\Omega \\ R_\Omega \end{Bmatrix} = \begin{bmatrix} \cos(\Theta_1)\cos(\Theta_2) & \sin(\Theta_2) & \sin(\Theta_1)\cos(\Theta_2) \\ -\cos(\Theta_1)\sin(\Theta_2) & \cos(\Theta_2) & -\sin(\Theta_1)\sin(\Theta_2) \\ -\sin(\Theta_1) & 0 & \cos(\Theta_1) \end{bmatrix} \begin{Bmatrix} P \\ Q \\ R \end{Bmatrix} \tag{8}$$

The above equation is not actually needed because P_Ω is equivalent to the magnitude of the rotational velocity vector leaving the other two components equal to zero. However, since the corrective damping moment is applied to the x-rotational axis, the inverse transformation matrix is needed to determine the moments with respect to the body axes. The full relation is shown in Eq. 9 below. As in the other strategies, the damping is applied using the schedule in Figure 3 with the total angular rate on the x-axis of that figure.

$$\begin{Bmatrix} C_{l\_apply} \\ C_{m\_apply} \\ C_{n\_apply} \end{Bmatrix} = \begin{bmatrix} \cos(\Theta_1)\cos(\Theta_2) & -\cos(\Theta_1)\sin(\Theta_2) & -\sin(\Theta_1) \\ \sin(\Theta_2) & \cos(\Theta_2) & 0 \\ \sin(\Theta_1)\cos(\Theta_2)) & -\sin(\Theta_1)\sin(\Theta_2) & \cos(\Theta_1) \end{bmatrix} \begin{Bmatrix} C_{apply} \\ 0 \\ 0 \end{Bmatrix} \tag{9}$$

As in the case of wind axis damping, Cm_apply must be multiplied by b/c before adding to the total aerodynamic pitching moment coefficient.

A.5 Angular Momentum Axis Damping

The angular momentum axis is the angular momentum vector of the aircraft. The simplest way to envision the angular momentum vector is to consider taking the angular velocity components (about principal axes), P, Q and R, and re-scale them by the (principal) moments-of-inertia of their respective axes (I_{xx}, I_{yy}, and I_{zz}). These re-scaled components form the components of another vector which is the angular momentum vector. This is illustrated in Figure 7 which portrays the unit rotational and momentum vectors at a particular instant in time.

As with the rotational axes, the momentum axes must first be defined in a convenient manner in order to develop a numerical procedure for implementing a momentum axis damping scheme. Equations 10 through 12 form the basis for determining the momentum axes. The equations below assume the use of principal axes so that the products of inertia are zero. The more general case requires the vector product of the inertia tensor with the angular velocity vector. For most aircraft, the body and principal axes are nearly coincident so that simply neglecting all of the products-of-inertia is a reasonable assumption.

$$\begin{aligned} H_x &= P * I_{xx} \\ H_y &= Q * I_{yy} \\ H_z &= R * I_{zz} \\ H &= \sqrt{H_x^2 + H_y^2 + H_z^2} \end{aligned} \tag{10}$$

$$\begin{aligned} \Theta_1 &\equiv \tan^{-1}\left(\frac{H_z}{H_x}\right) \quad . \; . \quad -\pi < \Theta_1 \le \pi \\ \Theta_2 &\equiv \sin^{-1}\left(\frac{H_y}{H}\right) \quad . \; . \quad -\frac{\pi}{2} < \Theta_2 \le \frac{\pi}{2} \end{aligned} \tag{11}$$

As in the rotational velocity damping scheme, for convenience the body 231 ($-\Theta_1$, Θ_2, 0) sequence is chosen.

$$\begin{Bmatrix} P_H \\ Q_H \\ R_H \end{Bmatrix} = \begin{bmatrix} \cos(\Theta_1)\cos(\Theta_2) & \sin(\Theta_2) & \sin(\Theta_1)\cos(\Theta_2) \\ -\cos(\Theta_1)\sin(\Theta_2) & \cos(\Theta_2) & -\sin(\Theta_1)\sin(\Theta_2) \\ -\sin(\Theta_1) & 0 & \cos(\Theta_1) \end{bmatrix} \begin{Bmatrix} P \\ Q \\ R \end{Bmatrix} \tag{11}$$

Once again, it is the transpose of the transformation in Eq. 11 which is actually needed to transform the damping moment back into the body axes. This full relation is given by Eq. 12 below. The damping moment is applied using Figure 3 with the total angular velocity (omega) on the x axis of that figure. Omega is used simply for convenience. Again, Cm_apply must be multiplied by: b/c to bring into standard form.

$$\begin{Bmatrix} C_{l\_apply} \\ C_{m\_apply} \\ C_{n\_apply} \end{Bmatrix} = \begin{bmatrix} \cos(\Theta_1)\cos(\Theta_2) & -\cos(\Theta_1)\sin(\Theta_2) & -\sin(\Theta_1) \\ \sin(\Theta_2) & \cos(\Theta_2) & 0 \\ \sin(\Theta_1)\cos(\Theta_2) & -\sin(\Theta_1)\sin(\Theta_2) & \cos(\Theta_1) \end{bmatrix} \begin{Bmatrix} C_{apply} \\ 0 \\ 0 \end{Bmatrix} \tag{12}$$

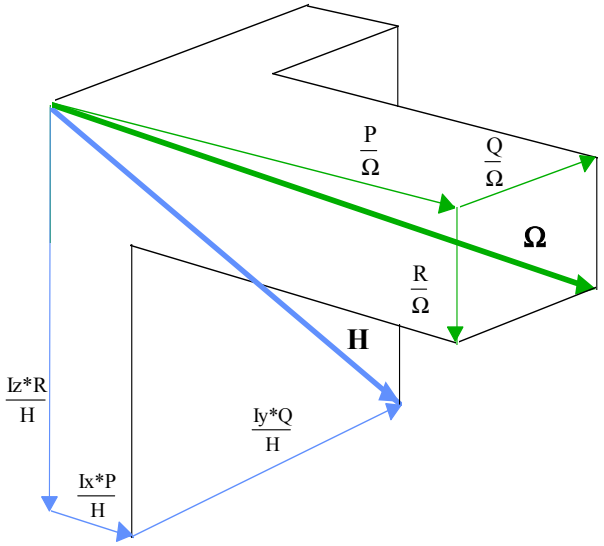

Figure 7. Relationship Between Angular Momentum and Angular Velocity Unit Vectors